Cerebral Cortex, December 2017;27: 5663–5671

doi: 10.1093/cercor/bhw336
Advance Access Publication Date: 22 November 2016
Original Article

ORIGINAL ARTICLE

Sequential Firing Codes for Time in Rodent Medial Prefrontal Cortex

Zoran Tiganj[1], Min Whan Jung[2,3], Jieun Kim[2], and Marc W. Howard[1]

[1]Department of Psychological and Brain Sciences, Center for Memory and Brain, Boston University, Boston, MA USA, [2]Center for Synaptic Brain Dysfunctions, Institute for Basic Science, Daejeon, Korea and [3]Department of Biological Sciences, Korea Advanced Institute of Science and Technology, Daejeon, Korea

Address correspondence to Zoran Tiganj. Email: zorant@bu.edu

Abstract

A subset of hippocampal neurons, known as "time cells" fire sequentially for circumscribed periods of time within a delay interval. We investigated whether medial prefrontal cortex (mPFC) also contains time cells and whether their qualitative properties differ from those in the hippocampus and striatum. We studied the firing correlates of neurons in the rodent mPFC during a temporal discrimination task. On each trial, the animals waited for a few seconds in the stem of a T-maze. A subpopulation of units fired in a sequence consistently across trials for a circumscribed period during the delay interval. These sequentially activated time cells showed temporal accuracy that decreased as time passed as measured by both the width of their firing fields and the number of cells that fired at a particular part of the interval. The firing dynamics of the time cells was significantly better explained with the elapse of time than with the animals' position and velocity. The findings observed here in the mPFC are consistent with those previously reported in the hippocampus and striatum, suggesting that the sequentially activated time cells are not specific to these areas, but are part of a common representational motif across regions.

Key words: mPFC, sequential coding, time cells

Introduction

A variety of brain regions have been implicated in interval timing over the scale of seconds to minutes, including the striatum (see Buhusi and Meck 2005 for a review) and medial prefrontal cortex (mPFC) (Mangels et al. 1998; Onoe et al. 2001; Kim et al. 2009). For instance, Kim et al. (2013) recently showed that the ensemble state in the mPFC changed gradually during the delay period of a temporal discrimination task. Critically, Kim et al. (2013) found that the discriminability of the time during the delay that could be computed from the ensemble neuronal activity decreased with time elapsed. Decreasing accuracy with elapsing time is a hallmark of behavioral measures of memory and timing in both human and nonhuman animals (Lejeune and Wearden 2006; Wearden and Lejeune 2008; Lewis and Miall 2009).

There are many potential mechanisms that could cause a change in accuracy at the ensemble level as time elapses. For instance, a population of neurons whose firing rate changes monotonically as a function of the logarithm of the time during the delay would have this property; Kim et al. (2013) reported a population of units exhibiting this pattern of results. However, there are other alternatives as well. For instance, several labs have reported "time cells" in the hippocampus that fire during circumscribed parts of a delay period (Pastalkova et al. 2008; Gill et al. 2011; MacDonald et al. 2011; Kraus et al. 2013; Salz et al. 2016). Also, time cells were reported in the striatum (Adler et al. 2012; Mello et al. 2015). Different time cells fire at different times during the interval, enabling a population of time cells to generate a signal that could be used in interval timing. The width of time cells' firing fields increases with their time of peak firing (Kraus et al. 2013; Howard et al. 2014; Mello et al. 2015; Salz et al. 2016), suggesting that the population of time cells is less able to distinguish times later in the interval.

Similarly, the density of time fields decreases as a function of time (Kraus et al. 2013; Mello et al. 2015; Salz et al. 2016), having the same consequence on the ability to distinguish times later in the interval.

In this paper we report the results of analyses on the dataset initially reported in Kim et al. (2013). In particular, we study the cells that fired during circumscribed periods of time during the delay interval to determine if the mPFC contains a significant population of sequentially activated time cells and to determine if these cells code time in such a way that there is decreasing temporal accuracy as a function of time within the delay. This would suggest a connection with the hippocampal and striatal time code and demonstrate that sequentially activated time cells are not specific to the hippocampus and striatum.

Materials and Methods

Behavioral Tasks

As described in Kim et al. (2009) and Kim et al. (2013), 3 young male Sprague Dawley rats performed a temporal discrimination task on a modified T-maze (63 × 69 cm, elevated 30 cm from the floor; 8 cm wide track with 2.7 cm walls around the track except the central connecting bridge; see Fig. 1A). Experiments were performed in the dark phase of 12 h light/dark cycle. The animals were required to discriminate 6 different durations of time intervals into short or long periods to obtain water reward. A new trial began when the animal came back from either goal location (Fig. 1A, white circles) to the central arm via the lateral alley and broke the central photobeam (Fig. 1A, arrow). The beginning of a time interval was signaled by a brief auditory tone when the animal broke the central photobeam. The end of a time interval was signaled by lowering the central bridge that allowed the animal to navigate to either goal location. The animals performed 164–273 (mean ± standard deviation [SD], 230 ± 20) trials per session. Six time intervals of different durations, which were spaced evenly on a logarithmic scale, were presented in equal probability in a random order. The animal had to navigate to one designated goal (left, $n = 2$ animals; right, $n = 1$ animal) when a short (3018, 3310, or 3629ms) interval was presented, and navigate to the opposite goal when a long (3979, 4363, or 4784ms) interval was presented to obtain water reward. The animals were well trained in the task by the time unit recordings began (see Kim et al. 2009 for details). As reported in Kim et al. (2013), the animals chose the correct target in 80% of trials. In the present study, we analyzed only the data recorded during the delay intervals.

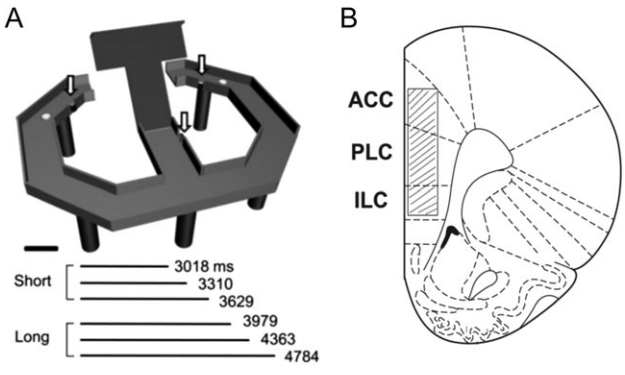

Figure 1. (*A*) Behavioral task. Rats were tested on a figure 8-shaped maze to choose between 2 target locations (white circles) depending on the duration of a given time interval. A time interval began when the animal broke the central photobeam (arrow). The connecting bridge was lowered at the end of the time interval allowing the animal to proceed to either goal location. The bridge was elevated again when the animal broke a photobeam (arrow) at either goal location. Scale bar, 10 cm. (*B*) Recording locations (shaded regions). The diagram is a coronal section view of the brain (2.7 mm anterior to bregma). Reproduced from Kim et al. (2013).

Unit Recording

As described in Kim et al. (2013), 12 tetrodes were chronically implanted in the left or right mPFC (2.7 mm anterior and 0.7 mm lateral to bregma) and unit signals were recorded from the dorsal anterior cingulate cortex (dACC), prelimbic cortex (PLC), and infralimbic cortex (ILC) (Fig. 1B). Each animals' head position was monitored by tracking a set of light-emitting diodes mounted on the headstage at 60 Hz. After completion of recordings, small marking lesions were made by passing an electrolytic current (50 mA, 30 s, cathodal) through one channel of each tetrode and recording locations were verified histologically. The anatomical location of each recorded unit was determined based on the location of a marking lesion and the advancement history of the corresponding tetrode. The recorded units were localized to the dACC (1.3–2.5 mm ventral to the brain surface), PLC (2.5–3.9 mm), and ILC (3.9–4.7 mm). A total of 993 well-isolated single units were recorded, 791 of which were classified as putative pyramidal cells. Of these, we eliminated 260 units with mean firing rate <1 Hz during the delay intervals. Additionally, in order to restrict our attention to units with spike waveforms that were stable over the recording sessions we eliminated 10 units with a difference of >10% in amplitude from the first to the last 5 min of each session. A total of 723 units contributed to the subsequent analyses.

Classification of Time Cells

Kim et al. (2013) reported a population of units that started firing prior to the initiation of the delay and decreased their firing as the delay proceeded and another population of units that increased their firing monotonically during the delay interval. Both groups of units could be responding to some event that preceded the delay interval or they could be predicting an event that follows the delay interval. In the present analyses, we restricted our attention to units that both increased and decreased the firing rate *within* the delay interval relative to a baseline, as defined more precisely later in this section. Unless otherwise stated, the analysis was done on the trials in which the animal completed the task successfully.

In order to evaluate to what extent the firing dynamics can be accounted for by the elapse of time we computed the maximum likelihood fit of the spike train given Gaussian-shaped time fields as well as behavioral correlates: position and speed. The fit was done on a spike train that included the activity during the delay intervals of all the trials when the longest delay interval (4784 ms) was presented. We restricted our attention to the longest delay intervals so that we could observe the temporal dynamics for as long as possible with this task. Given the duration of the delay intervals and the temporal resolution of 1 ms for each trial we had $N = 4784$ data points. If a spike was observed in a particular 1 ms time bin, then the corresponding data point was set to 1, otherwise it was set to 0.

We found the maximum likelihood of a spike train given the model with a set of parameters Θ. The model $p(t, \vec{r}(t)|\Theta)$ gives the probability of a spike at any given time point t:

$$p(t, \vec{r}(t)|\Theta) = a_1 + a_2T + a_3P + a_4S + a_5TP + a_6TS + a_7PS + a_8TPS. \quad (1)$$

The model takes into account the time $T(t; \sigma_t, \mu_t)$, the current position of the animal $P(\vec{r}(t); \vec{\sigma}, \vec{\mu}, \theta)$ and speed S, as well as their cross terms. Factors a_1 to a_8 determine the contribution of each of the terms, with a_1 being the constant term. The time term $T(t; \sigma_t, \mu_t)$ is a Gaussian-shaped time field defined as:

$$T(t; \sigma_t, \mu_t) = e^{\frac{-(t-\mu_t)^2}{2\sigma_t^2}}, \quad (2)$$

where μ_t is the temporal shift of the peak of the time field and σ_t is the standard deviation of the time field. The position term $P(\vec{r}(t); \vec{\sigma}, \vec{\mu}, \theta)$ is a Gaussian-shaped elliptical place field defined as:

$$P(\vec{r}(t); \vec{\sigma}, \vec{\mu}, \theta) = e^{-(\alpha(x-\mu_x)^2 - 2\beta(x-\mu_x)(y-\mu_y) + \gamma(y-\mu_y)^2)}. \quad (3)$$

In the above equation P is a function of $\vec{r}(t) = \{x(t), y(t)\}$, $\vec{\sigma} = \{\sigma_x, \sigma_y\}$ and $\vec{\mu} = \{\mu_x, \mu_y\}$. α, β, and γ are functions of θ, $\vec{\sigma}$, and $\vec{\mu}$ as follows: $\alpha = \cos^2(\theta)/2\sigma_x^2 + \sin^2(\theta)/2\sigma_y^2$, $\beta = -\sin(2\theta)/4\sigma_x^2 + \sin(2\theta)/4\sigma_y^2$, and $\gamma = \sin^2(\theta)/2\sigma_x^2 + \cos^2(\theta)/2\sigma_y^2$. $x(t)$ and $y(t)$ are the spatial coordinates of the animal's position as a function of time, μ_x and μ_y are the spatial shifts of the peak of the place field in the x and y direction, respectively, σ_x and σ_y are the standard deviations of the place field, also in the x and y direction, respectively, and θ is the angle of the place field.

The mean of the time term μ_t was allowed to vary between −100 ms and 4884 ms and the standard deviation σ_t varied between 0 and 10 s. The upper bounds of the spatial parameters were chosen such that they go well beyond the dimensions of the waiting area. In order to obtain a probability of a spike at any time bin we had to ensure that the values of $p(t, \vec{r}(t)|\Theta)$ are bounded between 0 and 1. Therefore, the coefficients were bounded such that $\sum_{i=1}^{8} a_i \leq 1$. The likelihood of the fit is defined as a product of these probabilities across all $N = 4784$ time bins within each trial and across M trials. We expressed the likelihood in terms of the negative log-likelihood (nLL), therefore instead of a product, a sum of the probabilities was computed:

$$\arg\min_{\Theta} \text{nLL} = -\sum_{\text{trial}} \sum_{t} \left[f_t \log(p_t) + (1 - f_t)\log(1 - p_t) \right]. \quad (4)$$

To find the best fitting model, the parameter space was iteratively searched using a combination of particle swarming and the Quasi-Newton method. Particle swarming was performed first (with the swarm size equal to 50) and its output was used to initialize the Quasi-Newton method which was performed second (the number of maximum function evaluations was set to 10 000). The computations were implemented in Matlab 2015b. To avoid solutions that converge to a local minimum, the fitting procedure was repeated until the algorithm did not result in better likelihood for at least 20 consecutive runs.

In order to quantify whether the contribution of the terms that contained time was significant, the maximum log-likelihood was computed again, but this time by setting the 4 time-related terms (a_2, a_5, a_6, a_8) to zero. So only: a_1, a_3, a_4, a_7, σ, μ and θ had to be estimated. Since the models with and without time are nested, the likelihood-ratio test was used to assess the probability that adding the time terms significantly improves the fit. The test is based on the ratio of the likelihoods of 2 different models and expresses how many times the data are more likely under one model than the other. For example, if the ratio of the likelihoods is 20, it means that one model is 20 times more likely than the other. Since the maximum likelihood fitting procedure gives us goodness of fit for different models in terms of likelihood, the likelihood ratio test was suitable to compare the models and assess statistical significance. To assure that a cell will not be classified as a time cell only due to its activity in a single trial, the analysis was done separately on even and odd trials. For a cell to be classified as a time cell, it was required that the likelihood-ratio test was significant ($P < 0.05$) for both even and odd trials. In order to eliminate cells with ramping or decaying firing rate during a delay interval, μ_t was required to be within the delay interval and at least one σ_t away from either the beginning or the end of the interval. Also, to eliminate cells with overly flat firing rate, σ_t was required to be at most equal to the length of the delay interval. To ensure reproducibility, the entire fitting procedure was done twice and exactly the same set of cells was classified as time cells in both runs.

Results

Sequentially Activated Time Cells Exist in mPFC

We identified a subpopulation of sequentially activated cells that fired at a consistent, circumscribed time during delay intervals (Fig. 2). These mPFC units appear to have firing correlates that resemble time cells observed in the hippocampus (Pastalkova et al. 2008; Gill et al. 2011; MacDonald et al. 2011; Kraus et al. 2013; Modi et al. 2014) and striatum (Adler et al. 2012; Mello et al. 2015). A total of 73/723 units were classified as time cells.

First, we note informally that the population of time cells decreased in its temporal accuracy as time during the interval proceeds. Figure 4A,C shows the ensemble similarity (cosine of the normalized firing rate vectors) of the population of time cells between all pairs of time points during the delay period (in Fig. 4C the firing that could be explained with position and speed was subtracted from the overall firing rate). This finding replicates the conclusions of Kim et al. (2013) but restricting attention to the population of time cells. Further analyses revealed 2 causes for the decrease in temporal accuracy. These can be read off from Figure 4B which shows the temporal profile of all 73 units classified as time cells, sorted by the peak time of the estimated Gaussian-shaped time field (μ_t), Again, similar results were obtained with only the firing that could not be explained by position and speed (Fig. 4D).

The Width of Firing Fields Increased with the Passage of Time

The width of the central ridge in Figure 4B,D increases from the left of the plot to the right of the plot. This suggests that units that had elevated firing rate earlier in the delay interval tend to have narrower time fields than the units that fire later in the delay interval. This impression was confirmed by analyses of the across-units relationship between the peak time (μ_t) and the standard deviation (σ_t) of the estimated Gaussian-shaped time fields across time cells (Fig. 3A). The correlation between the peak time and the width was significant (Pearson's correlation 0.52, $P < 10^{-5}$). Linear regression model linking the peak time (independent variable) and the width (dependent variable) resulted in a significant intercept equal to 0.27 ± 0.07 (SE) with $P < 0.001$ and a significant slope equal to 0.18 ± 0.04 (SE) with $P < 10^{-5}$.

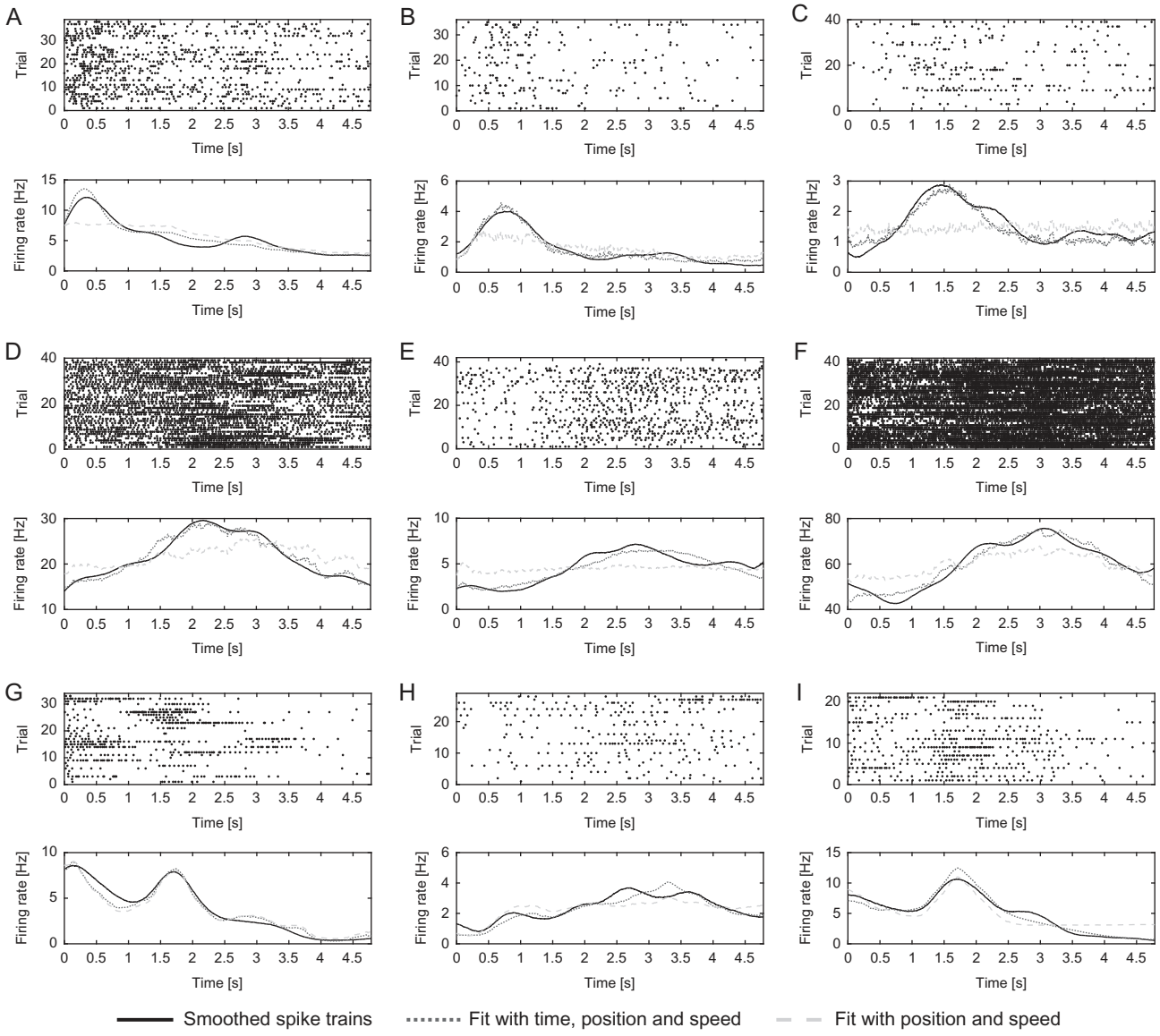

Figure 2. Firing properties of several time-modulated mPFC cells during the longest delay interval and the model fits with and without the temporal terms. Top 2 rows (*A–F*): examples of cells classified as time cells. The model that includes time component fits the spike train significantly better than the model that includes only position and speed. Bottom row (*G–I*): examples of cells that were not classified as time cells because behavioral correlates could account for the temporally modulated firing. Adding the time component to the model did not improve the fit significantly as compared with the model that contained only position and speed, despite the temporal modulation of the cell's activity. Each of the 9 plots (*A–I*) displays activity of a single cell. On each plot, the top row shows raster plot where each dot denotes a spike and the bottom row shows the averaged trial activity (solid line). Only trials when the animal made a correct choice are shown. The onset of the delay interval is at zero and the end at 4.784 s. The cells (*A–F*) are ordered such that the estimated peak time (μ_t) increases progressively from the first to the sixth cell.

Increase of the Width of the Time Fields with the Peak Time Was Not an Artifact of Trial Averaging

The property of spreading time fields seen in Figure 4 could be an averaging artifact caused by trial to trial variability. To show that this was unlikely to be the case we found the maximum likelihood fit for each trial independently. Prior to the fitting procedure all the parameters except μ_t and σ_t were fixed to the values found through the fit of the entire spike train spanning all the trials. The trial-averaged μ_t and σ_t were still significantly correlated (Pearson's correlation 0.42, $P < 10^{-3}$). This suggests that the dynamics of the spreading time fields is noticeable on a trial level as well. The trial-averaged and global (used in the previous analysis) μ_t and σ_t were significantly correlated (Pearson's correlation 0.80, $P < 10^{-16}$ for μ_t and 0.83, $P < 10^{-18}$ for σ_t).

Later Times Are Represented by Fewer Cells than Earlier Times

The population of cells covered the entire delay interval, but not evenly. The number of cells with peak firing later in the interval was smaller than the number of cells with peak firing earlier in the interval. This can be seen from the fact that the central ridge does not follow a straight line, as would have been expected of a uniform distribution of peak times (μ_t), but flattens as the interval proceeds. To quantify this, we examined

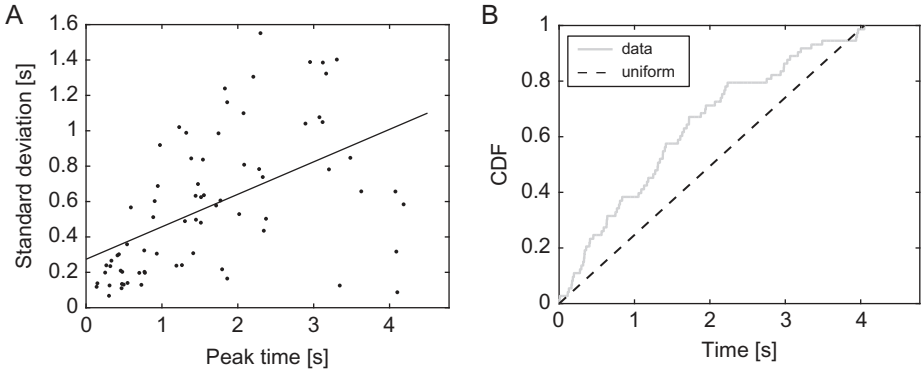

Figure 3. Sequentially activated time cells in mPFC encode time in a gradually decreasing fashion: 1) width of the time fields increases with the peak time (plot *A*, each dot represents a single time cell and the line is a least square fit linear fit without a constant term) and 2) peak times of the time fields are nonuniformly distributed along the delay interval; more cells had time fields earlier in the delay interval than later in the delay interval (plot *B*).

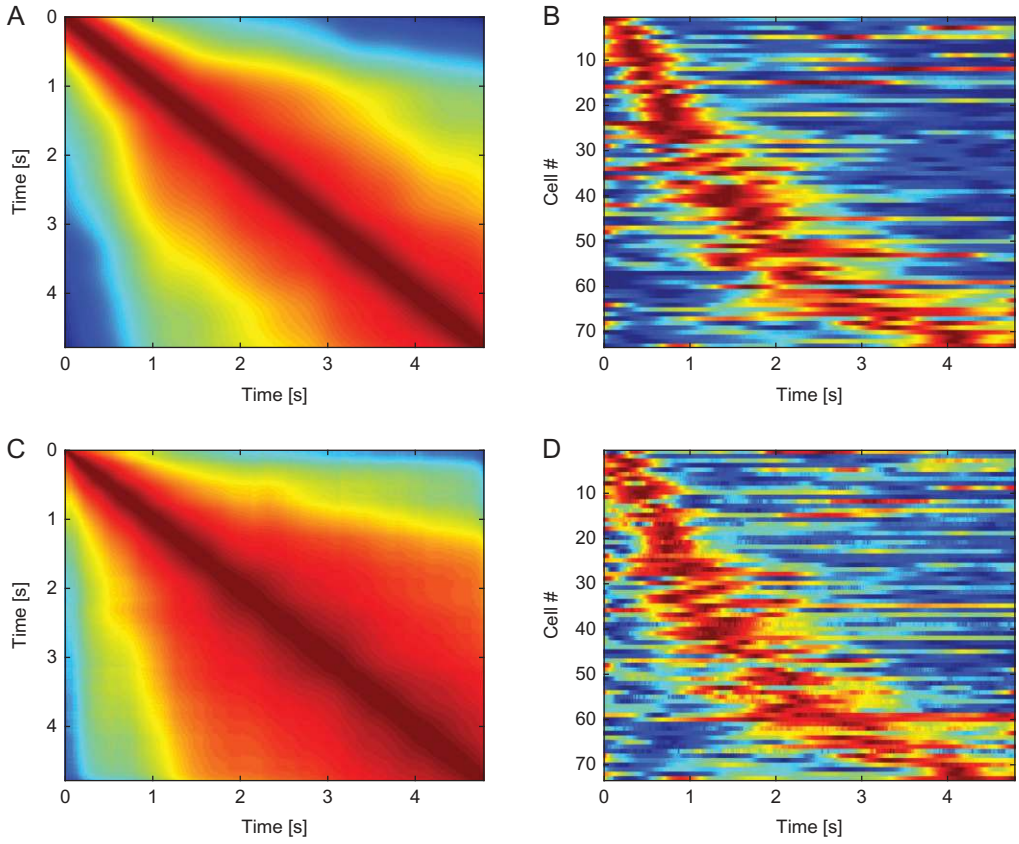

Figure 4. mPFC time fields show decreasing temporal accuracy for events further in the past. (*A*) Ensemble similarity of all 73 time cells given through a cosine of the angle between normalized firing rate population vectors. The angle is computed at all pairs of time points during the delay period. The bins along the diagonal are necessarily one (warmest color). The similarity spreads out indicating that the representation changes more slowly later in the delay period than it does earlier in the delay period. (*B*) Activity of all 73 time cells during the longest delay interval. Each row on the heatplot corresponds to a single cell and displays the firing rate (normalized to 1) averaged across all correct trials the animals performed during the longest delay interval. Red corresponds to high firing rate, while blue corresponds to low firing rate. The cells are sorted with respect to the peak time of the estimated Gaussian-shaped time fields (μ_t). There are 2 features related to temporal accuracy that can be seen from examination of this plot. First, time fields later in the delay are more broad than time fields earlier in the delay. This can be seen as the widening of the central ridge as the peak moves to the right. In addition, the peak times of the time cells were not evenly distributed across the delay, with later time periods represented by fewer cells than early time periods. This can be seen in the curvature of the central ridge; a uniform distribution of time fields would manifest as a straight line. (*C*,*D*) Same as (*A*) and (*B*) respectively, but only a part of the firing rate that was not accounted for by the behavioral correlates (position and speed) was used. (*E*) Same as (*B*), but for all the delay intervals when the animals made a correct choice (top row) or incorrect choice (bottom row). Vertical black lines mark the beginning (at time 0) and the end of a delay interval. Title of each heatplot contains a number of trials that the animals made in a particular condition. End of the delay interval seems to cause an abrupt change in the firing properties among the cells that were active at the time. Apart from that, there is no apparent qualitative difference among the 12 cases that could be attributed either to duration of the delay interval or to the correct or incorrect performance.

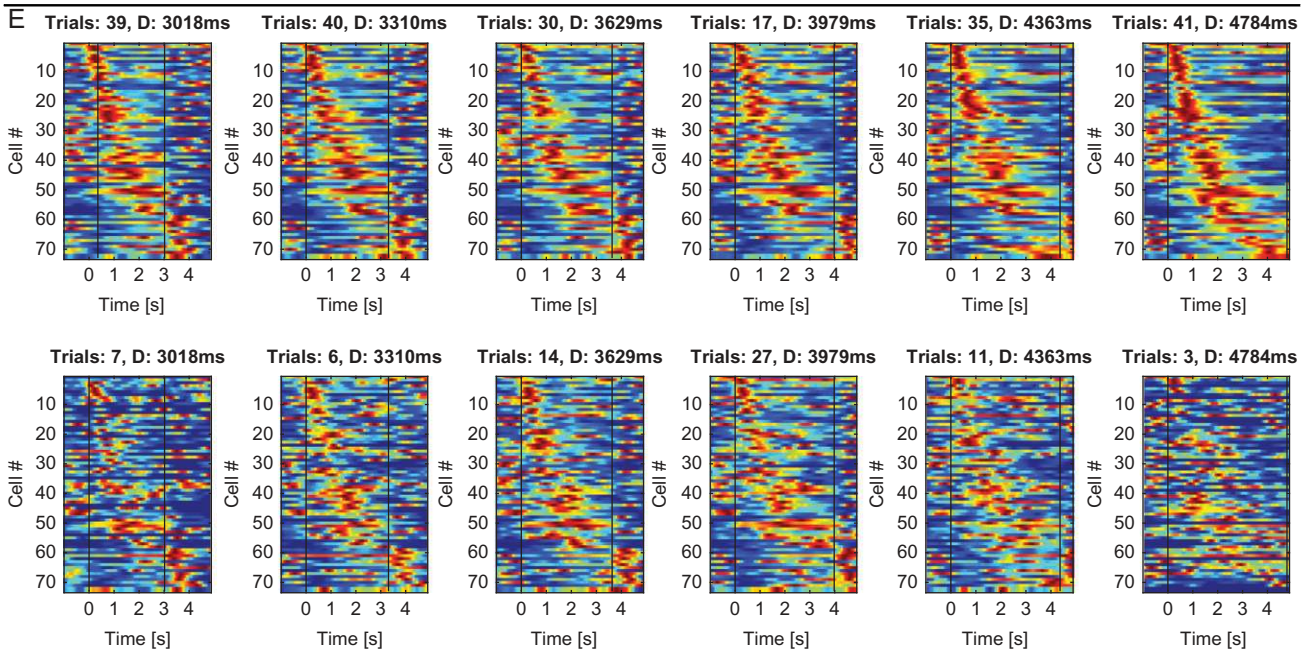

Figure 4. *Continued.*

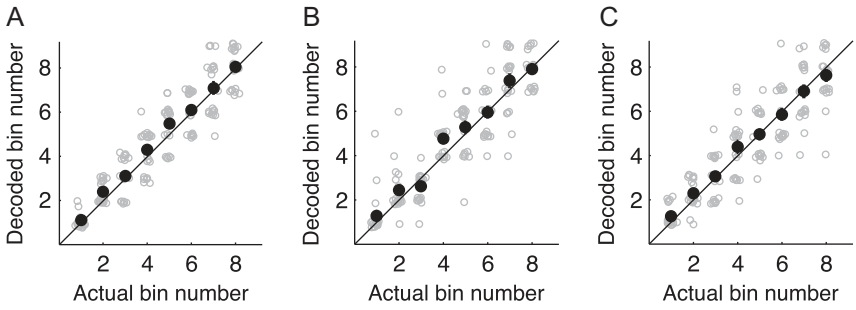

Figure 5. Time cells and ramping cells carried similar amounts of temporal information. Decoded bin number versus actual bin number. Open gray circles denote the trial-by-trial decoding results for each bin. Filled black circles and error bars denote their means and standard error of the mean (SEM) across trials. (*A*) Temporal decoding based on all 723 reported units. Mean error: 0.71 bins. (*B*) Temporal decoding based on all 73 time cells. Mean error: 0.74 bins. (*C*) Temporal decoding based on the randomly chosen 73 ramping cells. Mean error: 0.81 bins.

the distribution of the peak times across time cells (Fig. 3B). The KS test rejected the hypothesis that the distribution of the peak times is uniform (KS test $D(73) = 0.63$, $P < 10^{-12}$).

Comparing Time Cells in Different Subregions of the mPFC

We compared the time cells based on the subregion of the mPFC where they were recorded. The subregions that were considered were dACC, PLC, and ILC. The number of cells classified as time cells in dACC was 19 out of 120, in PLC 47 out of 426 and in ILC 7 out of 187. The proportion of time cells was not significantly different between dACC and PLC (Fisher's exact test $P > 0.15$, two-tailed), but it was significantly smaller in ILC with respect to both dACC (Fisher's exact test $P < 0.001$, two-tailed) and PLC (Fisher's exact test $P < 0.01$, two-tailed). Distributions of μ_t and σ_t did not significantly differ across the 3 subregions (Kruskal–Wallis test, for μ_t: $H = 1.86$, d.f. = 2, $P = 0.39$; for σ_t: $H = 2.31$, d.f. = 2, $P = 0.31$).

The Firing Fields Share Qualitative Properties Across the Delay Intervals of Different Duration

The animals were presented with 6 different delay intervals. In Figure 4E, the same type of a heatplot as on Figure 4B is shown, but for all 6 delay intervals when the animal made a correct choice (top row) and when the animal made an incorrect choice (bottom row). The cells are ordered in the same way as in Figure 4B. In general, the firing dynamics appeared to be abruptly interrupted once the end of the delay interval was signaled. The firing fields appear qualitatively similar regardless of the length of the delay interval or whether the animal made a correct or incorrect choice. Not enough error trials were available for a statistical comparison, especially at the extreme intervals.

mPFC Time Cells and Ramping Cells Convey Comparable Amount of Temporal Information

We quantified how well the mPFC neuronal ensemble kept track of time. The longest time interval (4784 ms) was divided into 10 equal-duration bins and the order of the middle 8 bins was decoded based on neural activity within each bin using linear discriminant analysis (Kim et al. 2013). We compared the results on different populations of cells: all 723 cells (Fig. 5A), all 73 time cells (Fig. 5B) and 73 ramping cells (selected randomly from a total of 228 cells that exhibit ramping firing rate by the criteria used in Kim et al. 2013, Fig. 5C). The mean error

in the prediction of elapsed time was similar for all 3 populations. This suggests that populations of time cells and ramping cells can convey roughly the same amount of information about the elapse of time.

Discussion

This study shows that mPFC contains sequentially activated time cells, similar to those previously reported in the hippocampus and striatum. As evaluated through ML fit, the findings were not attributable to confounds with position nor speed during the delay. The time fields of these units spanned the entire 5-s delay interval, but with temporal accuracy that decreased as time elapsed. The width of the time fields increased with temporal distance from the onset of the delay period and the distribution of the firing rate peaks strongly deviated from the uniform such that more units represented time periods early in the delay than later in the delay. These findings were not a result of a trial averaging artifact; rather the relationship between width and time was observed within single trials.

A Common Representational Motif for Time in the mPFC, Hippocampus, and Striatum

Our findings add to a literature on temporally modulated firing. Over longer scales, extensive evidence shows that the pattern of firing changes gradually over long periods of time in the hippocampus (Manns et al. 2007; Mankin et al. 2012, 2015) and mPFC (Hyman et al. 2012). This paper reports that mPFC contained sequentially activated time cells with decreasing temporal accuracy over shorter time scale. Several previous studies have found cells that fire for circumscribed periods of time during delay intervals in the hippocampus (Pastalkova et al. 2008; Gill et al. 2011; MacDonald et al. 2011; Naya and Suzuki 2011; Kraus et al. 2013; MacDonald et al. 2013; Modi et al. 2014; Salz et al. 2016) and the striatum (Adler et al. 2012; Mello et al. 2015). Many of these studies have observed decreasing temporal accuracy as a function of delay, due to spread in time field width (Adler et al. 2012; Kraus et al. 2013; Howard et al. 2014; Mello et al. 2015; Salz et al. 2016) and/or due to a nonuniform distribution of time field locations (Kraus et al. 2013; Mello et al. 2015; Salz et al. 2016). Despite differences in the procedures of the experiments, including variations in the behavioral task, the species, and the recording techniques, these remarkably consistent qualitative properties suggest a common motif for representation of time across these regions. In particular, resolution for the time of past events decreases with the passage of time. Notably, decreasing temporal resolution with the passage of time is a hallmark of behavioral findings from both timing tasks (Gibbon 1977; Wearden and Lejeune 2008; Lewis and Miall 2009) and a wide range of memory tasks across species (Gallistel and Gibbon 2000; Howard et al. 2015).

In addition to its hypothesized role in timing, the mPFC is known for its role in cognitive control (see for instance Miller and Cohen 2001) and working memory (see for instance Goldman-Rakic 1991, Miller et al. 1996, Euston et al. 2012). Time cells could be important in supporting these roles of the mPFC. If time cells were stimulus specific, they could maintain a dynamical representation of working memory in the form of a neural timeline, allowing construction of temporally structured associations (Howard et al. 2014). Such timeline would enable a direct readout of what happened when in the recent past, and potentially plays an important role in cognitive control. In particular, temporal associations across the stimulus space could be useful for learning rules that depend on the temporal spacing of the stimuli which could be used to exert causal control. The existing empirical evidence supports the hypothesis that the same population of neurons might be carrying information about both the elapsed time and stimulus identity (Romo et al. 1999; Matell et al. 2005). This has motivated the development of dynamical neural models that can account for this type of memory (Miller et al. 2003; Singh and Eliasmith 2006; Machens et al. 2010). In the present study, we could not test the stimulus specificity since the delay intervals always started with the same stimulus, thus finding empirical evidence for stimulus-specific time cells remains a challenge for future studies.

Mechanisms that Could Generate Time Cells

Time of the peak firing rate of the time cells typically exceeds the time constants of ion channels and neural processes, such as calcium clearance, which are both in general below 1 s. Several studies have proposed that neural firing with long time constants could be a result of feedback mechanisms at the single neuron level (Shouval and Gavornik 2011; Tiganj et al. 2015). For instance, one action potential could trigger the next through neuron-level processes that occur during action potential generation, such as calcium influx. Network-based mechanisms that can result in long time constants were also proposed (e.g., Bernacchia et al. 2011; Gavornik and Shouval 2011; Simen et al. 2011; Brody et al. 2003; Major and Tank 2004). Gradually changing firing rates with long time constants can be converted into time fields through a mechanism that resembles lateral inhibition (Howard et al. 2014). The mechanism would require 2 layer feed-forward network to construct time cells, which are not mutually connected. Alternatively, sequential activation (Jensen and Lisman 1996; Tieu et al. 1999; Hasselmo 2009; Itskov et al. 2011) could as well give rise to time cells. Spectral timing could also give rise to time cells (Grossberg and Schmajuk 1989; Grossberg and Merrill 1992). In general, proposed mechanisms should account for the qualitative properties observed here and in other studies: nonuniform distribution of the times of the peak firing rate and spread of the firing fields.

Relevance of Time Cells in Extracting Temporal Information

Time cells provide direct readout of the elapsed time, without the need for a decoding mechanism as in the case of other temporally modulated firing. An analogy for this type of coding could be found in the well known place code. Spatial position could be encoded through the firing rate of only 2 cells (if the firing rate would be proportional to the x and y position). However, place fields seem to cover the entire space providing a direct readout, such that spatial information is encoded through the identity of cells that are active at a given time. Similarly, time cells may provide information about the elapsed time through the identity of the currently active cells, rather than through a scalar value of the firing rate. This in turn can account for building temporal associations across the stimulus space as illustrated in Howard et al. (2014). Time cells and ramping cells convey comparable amounts of temporal information. It might be that the 2 populations encode the temporal information for different purposes. For instance, the purpose of time cells could be to construct a dynamical memory representation of what happened when, while ramping cells could play a role in decision making (Simen et al. 2011). Alternatively, a population of ramping cells with a spectrum of time constants

might be needed for the emergence of sequentially activated time cells (Howard et al. 2014).

Concluding Remarks

Previous work has shown that neural ensembles in the rodent mPFC code time with decreasing temporal accuracy (Kim et al. 2013). This paper extends these findings and reports that a subpopulation of units in the mPFC fired like sequentially activated time cells, firing for circumscribed periods of time during the delay of an interval discrimination task. These time cells exhibited decreasing temporal accuracy in 2 ways. First, time cells that fired later in the delay interval had wider temporal receptive fields than time cells that fired earlier in the delay. Second, the distribution of time fields was not uniform. More cells had time fields earlier in the delay period than later in the delay period. Taken together, these findings are consistent with the hypothesis that the mPFC is part of a system that represents time with decreasing accuracy over a scale of seconds.

Funding

NIMH 1R01MH112169, NIBIB R01EB022864, Office of Naval Research MURI N00014-16-1-2832, BU's Initiative for the Physics and Mathematics of Neural Systems, National Science Foundation PHY 1444389, and Research Center Program of the Institute for Basic Science (IBS-R002-G1).

Notes

Conflict of Interest: None declared.

References

Adler A, Katabi S, Finkes I, Israel Z, Prut Y, Bergman H. 2012. Temporal convergence of dynamic cell assemblies in the striato-pallidal network. J Neurosci. 32(7):2473–2484. 10.1523/JNEUROSCI.4830-11.2012.

Bernacchia A, Seo H, Lee D, Wang XJ. 2011. A reservoir of time constants for memory traces in cortical neurons. Nat Neurosci. 14(3):366–372.

Brody CD, Romo R, Kepecs A. 2003. Basic mechanisms for graded persistent activity: discrete attractors, continuous attractors, and dynamic representations. Curr Opin Neurobiol. 13(2):204–211.

Buhusi CV, Meck WH. 2005. What makes us tick? Functional and neural mechanisms of interval timing. Nat Rev Neurosci. 6(10):755–765. 10.1038/nrn1764.

Euston DR, Gruber AJ, McNaughton BL. 2012. The role of medial prefrontal cortex in memory and decision making. Neuron. 76(6):1057–1070.

Gallistel CR, Gibbon J. 2000. Time, rate, and conditioning. Psychol Rev. 107(2):289–344.

Gavornik JP, Shouval HZ. 2011. A network of spiking neurons that can represent interval timing: mean field analysis. J Comput Neurosci. 30(2):501–513. 10.1007/s10827-010-0275-y.

Gibbon J. 1977. Scalar expectancy theory and Weber's law in animal timing. Psychol Rev. 84(3):279–325.

Gill PR, Mizumori SJY, Smith DM. 2011. Hippocampal episode fields develop with learning. Hippocampus. 21(11):1240–9. 10.1002/hipo.20832.

Goldman-Rakic PS. 1991. Cellular and circuit basis of working memory in prefrontal cortex of nonhuman primates. Prog Brain Res. 85:325–336.

Grossberg S, Merrill J. 1992. A neural network model of adaptively timed reinforcement learning and hippocampal dynamics. Cognit Brain Res. 1:3–38.

Grossberg S, Schmajuk N. 1989. Neural dynamics of adaptive timing and temporal discrimination during associative learning. Neural Netw. 2(2):79–102.

Hasselmo ME. 2009. A model of episodic memory: mental time travel along encoded trajectories using grid cells. Neurobiol Learn Mem. 92:559–573.

Howard MW, MacDonald CJ, Tiganj Z, Shankar KH, Du Q, Hasselmo ME, Eichenbaum H. 2014. A unified mathematical framework for coding time, space, and sequences in the hippocampal region. J Neurosci. 34(13):4692–4707. 10.1523/JNEUROSCI.5808-12.2014.

Howard MW, Shankar KH, Aue W, Criss AH. 2015. A distributed representation of internal time. Psychol Rev. 122(1):24–53. 10.1037/a0037840.

Hyman JM, Ma L, Balaguer-Ballester E, Durstewitz D, Seamans JK. 2012. Contextual encoding by ensembles of medial prefrontal cortex neurons. *Proc Natl Acad Sci USA* 109 5086–5091. 10.1073/pnas.1114415109.

Itskov V, Curto C, Pastalkova E, Buzsáki G. 2011. Cell assembly sequences arising from spike threshold adaptation keep track of time in the hippocampus. J Neurosci. 31(8):2828–2834.

Jensen O, Lisman JE. 1996. Hippocampal CA3 region predicts memory sequences: accounting for the phase precession of place cells. Learn Memory. 3:279–287.

Kim J, Ghim JW, Lee JH, Jung MW. 2013. Neural correlates of interval timing in rodent prefrontal cortex. J Neurosci. 33(34):13834–13847. 10.1523/JNEUROSCI.1443-13.2013.

Kim J, Jung AH, Byun J, Jo S, Jung MW. 2009. Inactivation of medial prefrontal cortex impairs time interval discrimination in rats. Front Behav Neurosci. 3.

Kraus BJ, Robinson RJ II, White JA, Eichenbaum H, Hasselmo ME. 2013. Hippocampal "time cells": time versus path integration. Neuron. 78(6):1090–1101. 10.1016/j.neuron.2013.04.015.

Lejeune H, Wearden JH. 2006. Scalar properties in animal timing: conformity and violations. Q J Exp Psychol. 59(11):1875–1908.

Lewis PA, Miall RC. 2009. The precision of temporal judgement: milliseconds, many minutes, and beyond. Philos Trans R Soc Lond B Biol Sci. 364(1525):1897–1905. 10.1098/rstb.2009.0020.

MacDonald CJ, Carrow S, Place R, Eichenbaum H. 2013. Distinct hippocampal time cell sequences represent odor memories immobilized rats. J Neurosci. 33(36):14607–14616.

MacDonald CJ, Lepage KQ, Eden UT, Eichenbaum H. 2011. Hippocampal 'time cells' bridge the gap in memory for discontiguous events. Neuron. 71:737–749.

Machens CK, Romo R, Brody CD. 2010. Functional, but not anatomical, separation of "what" and "when" in prefrontal cortex. J Neurosci. 30(1):350–360.

Major G, Tank D. 2004. Persistent neural activity: prevalence and mechanisms. Curr Opin Neurobiol. 14(6):675–684. 10.1016/j.conb.2004.10.017.

Mangels JA, Ivry RB, Shimizu N. 1998. Dissociable contributions of the prefrontal and neocerebellar cortex to time perception. Cognit Brain Res. 7(1).

Mankin EA, Diehl GW, Sparks FT, Leutgeb S, Leutgeb JK. 2015. Hippocampal CA2 activity patterns change over time to a larger extent than between spatial contexts. Neuron. 85(1):190–201.

Mankin EA, Sparks FT, Slayyeh B, Sutherland RJ, Leutgeb S, Leutgeb JK. 2012. Neuronal code for extended time in the hippocampus. Proc Natl Acad Sci. 109:19462–19467. 10.1073/pnas.1214107109.

Manns JR, Howard MW, Eichenbaum HB. 2007. Gradual changes in hippocampal activity support remembering the order of events. Neuron. 56(PMC2104541):530–540.

Matell MS, Meck WH, Lustig C. 2005. Not "just" a coincidence: frontal-striatal interactions in working memory and interval timing. Memory. 13(3–4):441–448.

Mello GBM, Soares S, Paton JJ. 2015. A scalable population code for time in the striatum. Curr Biol. 25(9):1113–1122.

Miller EK, Cohen JD. 2001. An integrative theory of prefrontal cortex function. Annu Rev Neurosci. 24:167–202.

Miller EK, Erickson CA, Desimone R. 1996. Neural mechanisms of visual working memory in prefrontal cortex of the macaque. J Neurosci. 16(16):5154–5167.

Miller P, Brody CD, Romo R, Wang XJ. 2003. A recurrent network model of somatosensory parametric working memory in the prefrontal cortex. Cereb Cortex. 13(11):1208–1218.

Modi NM, Ashesh DK, Bhalla SU 2014. CA1 cell activity sequences emerge after reorganization of network correlation structure during associative learning. eLife 3 0. http://dx.doi.org/10.7554/eLife.01982 10.7554/eLife.01982.

Naya Y, Suzuki W. 2011. Integrating what and when across the primate medial temporal lobe. Science. 333(6043):773–776.

Onoe H, Komori M, Onoe K, Takechi H, Tsukada H, Watanabe Y. 2001. Cortical networks recruited for time perception: a monkey positron emission tomography (PET) study. NeuroImage. 13(1):37–45.

Pastalkova E, Itskov V, Amarasingham A, Buzsaki G. 2008. Internally generated cell assembly sequences in the rat hippocampus. Science. 321(5894):1322–1327.

Romo R, Brody CD, Hernández A, Lemus L. 1999. Neuronal correlates of parametric working memory in the prefrontal cortex. Nature. 399(6735):470–473.

Salz DM, Tiganj Z, Khasnabish S, Kohley A, Sheehan D, Howard MW, Eichenbaum H. 2016. Time cells in hippocampal area CA3. Neurosci. 36(28):7476–7484.

Shouval HZ, Gavornik JP. 2011. A single spiking neuron that can represent interval timing: analysis, plasticity and multi-stability. J Comput Neurosci. 30(2):489–499. 10.1007/s10827-010-0273-0.

Simen P, Balci F, de Souza L, Cohen JD, Holmes P. 2011. A model of interval timing by neural integration. J Neurosci. 31(25):9238–9253. 10.1523/JNEUROSCI.3121-10.2011.

Singh R, Eliasmith C. 2006. Higher-dimensional neurons explain the tuning and dynamics of working memory cells. J Neurosci. 26(14):3667–3678.

Tieu KH, Keidel AL, McGann JP, Faulkner B, Brown TH. 1999. Perirhinal-amygdala circuit level computational model of temporal encoding in fear conditioning. Psychobiology. 27:1–25.

Tiganj Z, Hasselmo ME, Howard MW. 2015. A simple biophysically plausible model for long time constants in single neurons. Hippocampus. 25(1):27–37.

Wearden JH, Lejeune H. 2008. Scalar properties in human timing: conformity and violations. Q J Exp Psychol. 61(4):569–87.